Research Article

Norah Salem Alsaiari*, Majed Salem Alsaiari, Fatimah Mohammed Alzahrani, Abdelfattah Amari*, and Mohamed A. Tahoon

Synthesis, characterization, and application of the novel nanomagnet adsorbent for the removal of Cr(vI) ions

https://doi.org/10.1515/rams-2023-0145 received February 13, 2023; accepted October 24, 2023

Abstract: The synthesis of an efficient adsorbent to remove chromium ions from water is challenging. Therefore, in this study, a new nanomagnet composite (Fe₃O₄/biochar/ ZIF-8) was synthesized by a one-pot hydrothermal method using a metal-organic framework (MOF, ZIF-8) as a sacrificial template, citrus peels as a source of biochar, and iron oxide nanoparticles for magnetization. The synthesized nanocomposite showed a high efficiency toward the adsorption of Cr(v1) ions. The adsorption study showed that the experimental data were well-described using the Langmuir isotherm model and pseudo-second-order model. According to the Langmuir model, the adsorption capacities toward Cr(v1) adsorption were 77 and 125 mg·g⁻¹ for Fe₃O₄/biochar and Fe₃O₄/biochar/ZIF-8, respectively, indicating the role of MOF in improving the adsorption performance. The Fe₃O₄/biochar/ ZIF-8 showed an excellent adsorption performance in the presence of coexisting ions at a wide pH range using different eluents to study reusability up to five successive cycles. We can conclude from this study that this nanoadsorbent is a promising material for removing pollutants from environmental water samples.

Fatimah Mohammed Alzahrani: Department of Chemistry, College of Science, Princess Nourah bint Abdulrahman University, P.O. Box 84428, Riyadh 11671, Saudi Arabia

Mohamed A. Tahoon: Department of Chemistry, College of Science, King Khalid University, P.O. Box 9004, Abha 61413, Saudi Arabia; Chemistry Department, Faculty of Science, Mansoura University, Mansoura 35516, Egypt

Keywords: ZIF-8, nanocomposite, metal–organic framework

1 Introduction

The heavy metals, dyes, and pharmaceuticals pollution released from industrial effluents easily penetrate the water environment and cause a long-term threat to human and aquatic life. Particularly, dangerous heavy metals such as hexavalent chromium ions Cr(vi) cause severe problems [1]. Chromium (Cr) is a crucial element that is extensively used in a variety of sectors, including alloy production, leather tanning, and electroplating [2]. Naturally, chromium has two oxidation states, hexavalent and trivalent, of which the hexavalent state shows a higher toxicity due to its mutagenicity, carcinogenicity, and greater mobility [3]. On the other hand, the trivalent state can be utilized by the cell for many biological processes [4]. Therefore, the World Health Organization and environmental protection organizations in various nations have imposed tight restrictions on the amount of Cr ions in surface or drinking water [5,6]. As a result, it is now of utmost importance to effectively remove Cr(vi) ions from aqueous solutions. Several techniques have been applied for the removal of Cr(vi) ions from aqueous solutions such as ion exchange [7,8], membrane separation [9], phytoremediation [10], microbial remediation [11], and electrochemical reduction [12]. Adsorption technology is crucial in the removal of Cr(vi) ions owing to its exceptional advantages such as simplicity, high efficiency, cost-effectiveness, and flexibility [13] and uses a range of adsorbents, including carbon nanotubes [14,15], activated carbon [16], metal oxides [17], graphene oxide [18], and clay minerals [19]. However, the majority of adsorbents are not suitable for practical applications due to their poor selective characteristics and limited adsorption capabilities in hostile environments [20]. Therefore, the need for novel nanomaterials that can sustain strong adsorption performance in challenging practical environments is critical.

^{*} Corresponding author: Norah Salem Alsaiari, Department of Chemistry, College of Science, Princess Nourah bint Abdulrahman University, P.O. Box 84428, Riyadh 11671, Saudi Arabia, e-mail: nsalsaiari@pnu.edu.sa

^{*} Corresponding author: Abdelfattah Amari, Department of Chemical Engineering, College of Engineering, King Khalid University, P.O. Box 9004, Abha 61411, Saudi Arabia, e-mail: abdelfattah.amari@enig.rnu.tn Majed Salem Alsaiari: Department of Chemistry, College of Science, King Abdulaziz Military College, Riyadh 13952, Saudi Arabia

Metal-organic frameworks (MOFs) have attracted attention over the last few years due to their intriguing structural properties, such as variable pore size, programmable functionalities, abundant functional groups, and high specific surface areas [21]. These properties allowed their wide applications in different fields including environmental remediation [22], catalysis [23], supercapacitors [24], sensors [25], energy storage [26], and adsorption [27–30]. The zeolitic imidazolate framework-8 (ZIF-8) is a member of the MOF family of materials and has comparatively high thermal stability than other MOFs [31]. Through chelation interactions, the metal coordination site (Zn²⁺) in ZIF-8 may create metal complexes with the adsorbate, and the N heteroatom might enhance adsorption chelation sites [32]. However, the application of MOFs in water treatment is still restricted due to many factors such as the difficult and complicated recyclability of most MOFs, poor stability, and weak selectivity [33]. By encapsulating functional nanoparticles into MOFs, researchers can create MOFcontaining nanocomposites that combine the benefits of two different components and improve synergistic effects in the resulting hybrid products. Subsequently, MOFs must be modified to be widely used. Having the potential for regeneration and reuse, biochar is a novel type of environmentally friendly material that is rich in carbon [34]. It can be made from a variety of substances, including industrial biowastes, marine and aquatic species, and agricultural and forestry leftovers (such as wood chips, rice straw/husk, fruit peels, leafy litter, etc.) [35–38]. In recent years, biochar has attracted considerable interest as an adsorbent from environmental media because of its inexpensive cost, relatively high porosity, porous qualities, possibility of regeneration, and reuse. For instance, biochar from crab shells could efficiently remove dye from water [39], human hair-derived biochar is utilized to adsorb tetracycline antibiotics [40]. and biochar from coconut shells acts as an efficient adsorbent for the removal of methylene blue [41]. However, using traditional separation techniques like centrifugation, filtering, and gravity sedimentation to separate biochar is laborious, time-consuming, and expensive [42]. Subsequently, there is an urgent need for the magnetization of biochar to produce magnetic biochar adsorbent that exhibits a predominant future due to the easy separation using an external magnet instead of traditional methods [43]. For eliminating inorganic and organic contaminants from aquatic environments, magnetic biochar has been widely used. In general, ferric and ferrous compounds are used as precursors to precipitate and link magnetic media, such as zero-valent iron, magnetite (Fe₃O₄), and maghemite (γ -Fe₂O₃), onto biochar matrix [44,45]. With the addition of the biochar matrix and magnetic iron, the magnetic biochar typically displays a relatively high

adsorption capability and stability [46]. Since iron oxide is more oxidatively stable than zero-valent iron, iron oxidedoped magnetic biochar has many advantages for real-world use. Due to their strong magnetic and adsorptive properties, Fe₃O₄ and y-Fe₂O₃ are excellent candidates for the synthesis of iron oxide-doped magnetic biochar. Therefore, the preparation of MOF-magnetic biochar-based composites is a promising approach due to the ability to attain complementary effects between the 3-D MOFs and carbon-based materials. Due to the abundance of active sites, hierarchical porosity, and increased specific surface area, MOFs conjugated with biochar formed from naturally renewable biomass might significantly improve the physical and chemical performances of the biochar. The addition of biochar to the MOF can significantly enhance MOF agglomeration and increase the number of exposed active sites, which ultimately results in MOFs with a relatively high adsorption capacity and stability. Additionally, the recycling of adsorbents was aided by magnetic modification, and the ability of carbon-based materials to successfully prevent secondary contamination brought on by the dissolution of metal ions made them suitable for use in genuine largescale applications.

The novelty of this study is the synthesis of a new magnetically modified MOF-based nanocomposite from three different components having a porous architecture that was characterized and investigated for efficient water treatment. Herein, a novel magnetic ZIF-8/biochar nanocomposite was prepared and investigated for the removal of Cr (vi) ions from an aqueous solution. To assess the removal efficiencies under various conditions, batch adsorption tests were carried out, and the mechanisms were also investigated. The particular points were to synthesize and characterize magnetic ZIF-8/biochar nanocomposite, assess and compare the adsorption capacities toward Cr(v_I) ions using different adsorbents by studying the effect of key factors (pH and ionic strength) on adsorption capacity, explore the adsorption mechanisms through a series of experiments, such as kinetics, isotherms, and physicochemical characterization analysis, and investigate the regeneration and reusability of the adsorbent. The findings of this work would serve as a guide for the synthesis of functionalized biochar and the removal of Cr(vi) ions from contaminated water. It will also provide an effective approach for constructing new MOF-based adsorbents with excellent adsorption capacity, and attract MOF's attention for the water treatment. Furthermore, it will help researchers to overcome the limitations of using MOF-based materials as adsorbents such as poor mechanical stability, difficulty of connecting MOFs with matrix, poor reusability, and high water solubility.

2 Materials and methods

2.1 Chemicals

The citrus fruits as carbon precursors were bought from local supermarkets (Mansoura, Egypt). Zinc nitrate hexahydrate (Zn(NO₃)₂·6H₂O), 2-methylimidazole, and potassium hydroxide (KOH) were purchased from Sigma-Aldrich. Ammonium iron(III) sulfate dodecahydrate (NH₄Fe(SO₄)₂·12H₂O) was supplied by Shanghai Chemical Reagent Co., Ltd. (Shanghai, China). Ammonium ferrous sulfate ((NH₄)₂Fe(SO₄)₂·6H₂O) was obtained from Chongqing Beibei Chemical Reagent (Chongqing, China). Sodium hydroxide (NaOH), hydrochloric acid (HCl), potassium dichromate (K₂Cr₂O₇), etc. were obtained from Sinopharm Chemical Reagent Co., Ltd. China. All chemicals used were of analytical grade and used without any additional purifications. A stock solution of K₂Cr₂O₇ was prepared using distilled water and diluted for further experimental purposes.

2.2 Synthesis of ZIF-8

To synthesize MOFs (ZIF-8), the steps in Liu et al. [47] were followed with some modifications. Briefly, two separate volumes (40 mL) of methanol were used to dissolve Zn $(NO_3)_2 \cdot 6H_2O$ (0.587 g) and 2-methylimidazole (1.298 g). Then, the metal solution was stirred for 1 h under sonication. Finally, the ligand solution was added to the metal solution at room temperature with sonication.

2.3 KOH-activated-citrus peel powder

The carbon precursor was extracted from citrus peels. First, citrus peels that had been cleaned were chopped into pieces and dried at 80°C before being processed into powder. Then, KOH (30%) was used to activate the citrus peel powder in a ratio of 1:2 (W/V) to KOH. It was allowed to stand for 30 min before being dried for 3 h at 70°C in an oxygen-free environment.

2.4 Synthesis of Fe₃O₄ nanoparticles

The magnetic Fe₃O₄ nanoparticles were synthesized by the co-precipitation method as described in the literature [48]. Briefly, 300 mL of distilled water was used to disperse 3.36 g of $(NH_4)_2Fe(SO_4)_2 \cdot 6H_2O$ and 8.1 g of $NH_4Fe(SO_4)_2 \cdot 12H_2O$ at a temperature of 50°C under an N₂ atmosphere. Then, ammonium solution (20 mL, 8 mol·L⁻¹) was added drop by drop to the solution reaction to precipitate the magnetic particles. After that, the pH of the solution reaction was adjusted to 11 using NaOH solution under an ultrasonicator for 15 min. Using an external magnet, the precipitated product was separated and washed several times using distilled water until the pH of the filtrate became 7. Finally, the magnetic nanoparticles were dried at 45°C under a vacuum.

2.5 Synthesis of the magnetic ZIF-8/biochar nanocomposite

The nanocomposite of magnetic ZIF-8/biochar was synthesized by a one-pot hydrothermal method. Briefly, 100 mL of ZIF-8 suspensions were used to dissolve 10 g of Fe₃O₄ and KOH-activated citrus peel powder while stirring at room temperature for 13 h. After that, using an external magnet, the precipitate was collected and dried under a vacuum at 65°C. Then, the resulting product was inserted into a tube furnace for slow continuous pyrolysis under an N2 atmosphere at 600°C for 2 h using a rate of 5°C·min⁻¹. The product was dipped in HCl solution (1 M) after cooling to room temperature to remove the impurities and alkali. Then, the product was washed using ethyl alcohol and water several times until the pH of the filtrate reached 7. The resulting composite was then dried and ground. The synthesized nanocomposite magnetic ZIF-8/biochar was then stored for the next experiments. Additionally, the composite Fe₃O₄/biochar was synthesized using the typical steps but without adding the ZIF-8 MOF during the synthesis.

2.6 Batch adsorption experiments

The efficiency of synthesized adsorbents for the removal of Cr(vi) ions was evaluated using batch adsorption experiments. In brief, 20 mL of Cr(vi) solution in the concentration range of 0-500 mg·L⁻¹ was added to 0.05 g of adsorbent in a flask while the solution pH was 2. Using a shaking water bath, the solution was shaken for 24 h at 180 rpm. To study the kinetics of the adsorption process, 200 mL of 300 mg·L⁻¹ Cr(v_I) solution was added to 0.5 g of the adsorbent in a flask at pH 2 and the solution was shaken for 24 h at 180 rpm. Then, at different time intervals, part of the solution was withdrawn and analyzed for the presence of Cr(vi) ions and Cr using UV-vis spectrophotometer at

4 — Norah Salem Alsaiari et al. DE GRUYTER

 $\lambda = 540 \text{ nm}$ after a complex formation with 1,5-diphenylcarbazide with a flame atomic absorption spectrometer, respectively. The difference between total Cr and Cr(vi) ions is used to calculate the concentration of Cr(III) ions. Before each analysis and after the completion of the adsorption process, the adsorbent was collected using an external magnet. Additionally, the effect of different parameters on adsorption was investigated including ionic strength (0-0.1 M), pH (1:10), and 0.01 M competing ions (PO₄³⁻, SO₄²⁻, Cl⁻, Fe³⁺, Ca²⁺, and Na⁺). During these adsorption experiments, the solid/liquid ratio was fixed at 2.5 g·L⁻¹ (20 mL solution). Moreover, desorption and reusability were investigated using different eluents including NaOH, NaHCO₃, Na₂EDTA, HNO₃, and NaNO₃ at a concentration of 0.01 M. In this experiment, 20 mL of Cr(vi) solution at pH 2 and a concentration of 50 mg·L⁻¹ was mixed with the adsorbent, which was then collected with a magnet, washed with distilled water, and dipped in an eluent solution for 24 h to study the desorption efficiency. In the reusability experiment, the desorbed adsorbents using NaOH were used to adsorb Cr(vi) ions for five successive cycles to determine the adsorption capacity. All previously described adsorption experiments were performed in triplicate to approve the quality of results.

2.7 Characterization of synthesized adsorbents

To characterize the synthesized materials, different techniques have been used. The essential functional groups on the surface of synthesized materials were investigated using Fourier transform infrared spectroscopy (FT-IR; IRTracer-100 Shimadzu, Japan) in the range of 400–4,000 cm⁻¹. The magnetic behavior of materials was identified using a vibrating sample magnetometer (VSM; Lake Shore 7404, USA). The thermal gravimetric analysis (TGA; STA409PC, DSC404F3, Germany) was used to investigate the thermal stability of the synthesized materials under an N2 environment in the range of 30–1,000°C at a heating rate of 10°C·min⁻¹. Moreover, the surface morphology was investigated using a scanning electron microscope (SEM, Zeiss Genimi500, Zeiss, Germany). The Raman spectra were analyzed using a Raman spectrometer (Renishaw, UK). The specific surface area (S_{BET}) was determined using the Brunauer-Emmett-Teller method via the adsorption/desorption isotherms of N2 at a temperature of 77 K. The pH drift method was used to calculate the point of zero charge (pH_{PZC}) at which Δ pH = 0 (where Δ pH is the difference between the initial and final pH values).

3 Results and discussion

3.1 Characterization of the synthesized materials

To achieve the successful characterization of the synthesized materials, several common techniques have been applied. In this section, we used different techniques to verify the successful fabrication of the desired materials. First, the scanning electron microscope (SEM) was used to detect the morphologies of the synthesized materials and follow the surface change resulting from the added materials. Figure 1a shows the SEM image of the citrus peelderived biochar that appeared to have several pores on its rough structure surface. Figure 1b shows the SEM image of the Fe₃O₄/biochar composite in which the composite has a stacked and smooth structure surface holding several nanoparticles with diameters in the range of 25-30 nm. The appeared nanoparticles to confirm the successful precipitation of magnetic Fe₃O₄ nanoparticles on the surface of the biochar.

Figure 1c shows the SEM image of the Fe₃O₄/biochar/ ZIF-8 composite. Figure 1c shows that the introduction of the ZIF-8 MOF to the composite has a great effect on the structure, which is clearly shown via the morphology change. The Fe₃O₄/biochar/ZIF-8 composite appeared to have wrinkled edges with smooth surfaces and a multilayer structure, which could be the result of ZIF-8 decomposing at a higher pyrolysis temperature. Additionally, to sustain the framework, the partially decomposed ZIF-8 was distributed between the sheets that resemble graphene as a sacrifice template. Also, the crystallinity of the synthesized materials was studied using XRD patterns as shown in Figure 2a. According to the XRD patterns, the synthesized magnetic Fe₃O₄ nanoparticles showed the appearance of characteristic planes (440), (511), (422), (400), (311), and (220) at $2\theta = 62.9^{\circ}$, 57.2°, 53.7°, 43.4°, 35.5°, and 30.2°, respectively [49]. When the XRD patterns of the Fe₃O₄ nanoparticles and Fe₃O₄/biochar composite were compared, it was noticed that the crystallinity remained unchanged, which indicated the stability of the Fe₃O₄/biochar composite crystal structure even after loading of magnetic nanoparticles on the biochar surface. After the addition of the ZIF-8 MOF to the Fe₃O₄/biochar composite, several new peaks appeared, which were attributed to the addition of the MOF. The results of the XRD patterns revealed the crystal structures of the Fe₃O₄ nanoparticles and Fe₃O₄/biochar composite, suggesting that the synthesized Fe₃O₄/biochar/ ZIF-8 composite was well fabricated. The presence of functional groups and information about chemical bonding can

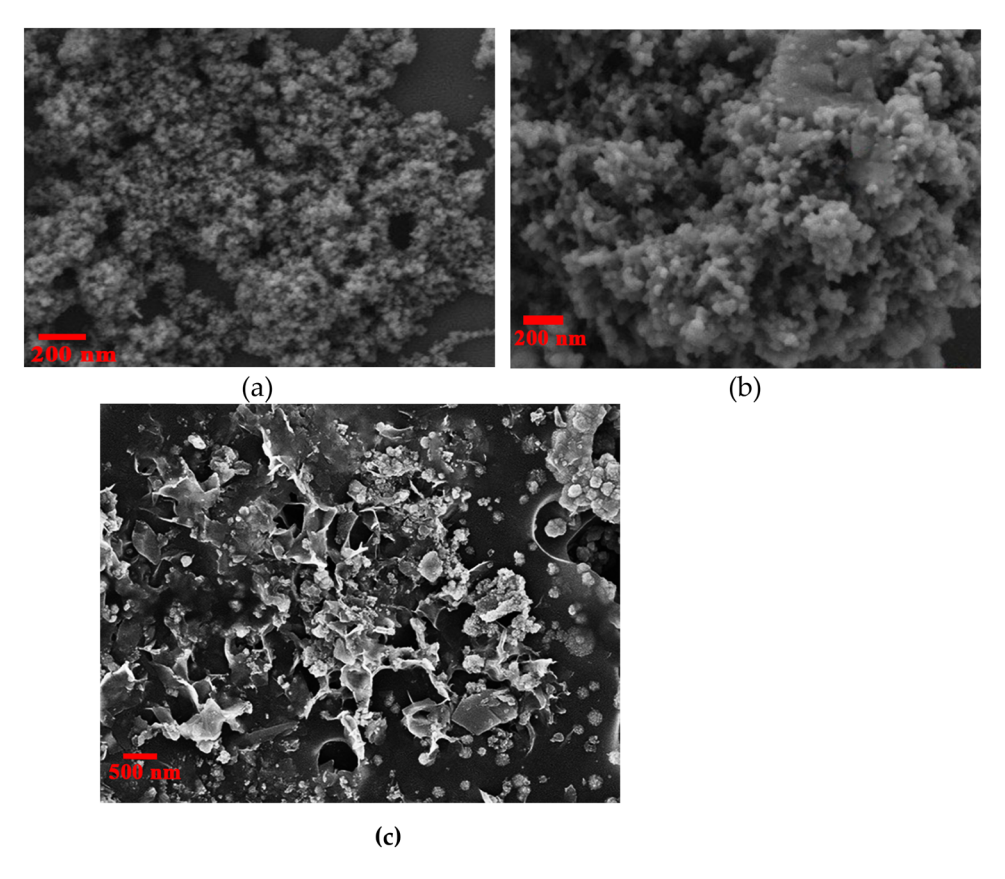


Figure 1: SEM images of the biochar (a), Fe₃O₄/biochar (b), and Fe₃O₄/biochar/ZIF-8 (c).

be obtained using FT-IR spectra, as shown in Figure 2b. Generally, the characteristic peak at 1,621 cm⁻¹ was attributed to the C=N bond in the ZIF-8 MOF or to the C=C bond in the aromatic ring. Also, the broad peaks at 3,421 cm⁻¹ were attributed to the N-H stretching vibration or the O-H stretching vibration [50,51]. Additionally, the C-O stretching vibration of carboxylic acids and aromatic ethers is usually represented by the band at 1,095 cm⁻¹. These oxygen-containing functional groups and double bonds of aromatic rings are very effective in pollutant removal via hydrogen bonding and π - π interactions, respectively [50,52,53]. Moreover, that ZIF-8 MOF was well introduced into the nanocomposite was confirmed from the appearance of the peak at 480 cm⁻¹ that was attributed to Zn-N vibrations [54]. Also, that Fe₃O₄ was well introduced into the nanocomposite was confirmed from the appearance of the peak at 568 cm⁻¹ that was attributed to Fe-O vibrations.

Furthermore, the Raman spectra of the synthesized materials are shown in Figure 2c. In Raman spectra, there are two bands G- and D-bands, which are attributed to the ordered graphitic sp² hybridized carbon and disordered sp3 hybridized carbon, respectively. The degree of graphitization can be obtained from the total peak area of the

Raman spectra [55]. As a result, it is possible to use the peak area rate from the D-band to the G-band (I_D/I_G) as a guideline when determining the degree of structural disorder in carbon materials [56]. According to Figure 2c, the $I_{\rm D}/I_{\rm G}$ of the Fe₃O₄/biochar is higher than that of the Fe₃O₄/biochar/ ZIF-8 nanocomposite, indicating the increase of sp²-hybridized domains. The Raman spectra results indicated the successful introduction of the ZIF-8 MOF to the composite Fe₃O₄/biochar. Additionally, the magnetic properties of the synthesized materials were investigated using VSM, as shown in Figure 3a. According to Figure 3a, Fe₃O₄, Fe₃O₄/biochar, and Fe₃O₄/biochar/ZIF-8 have excellent magnetic properties. The saturation magnetization values were 24.53, 32.30, and 67 emu·g⁻¹ for Fe₃O₄/biochar/ZIF-8, Fe₃O₄/biochar, and Fe₃O₄, respectively. According to the results, the saturation magnetization of pure Fe₃O₄ nanoparticles is the highest and this value was decreased after the incorporation of non-magnetic biochar and ZIF-8. However, by using an external magnet, these composites still exhibited magnetic properties and could be easily collected from the solution.

As the specific surface area is very important in determining the adsorption properties of the materials, the N_2 adsorption/desorption isotherm method was used for the

6 — Norah Salem Alsaiari et al. DE GRUYTER

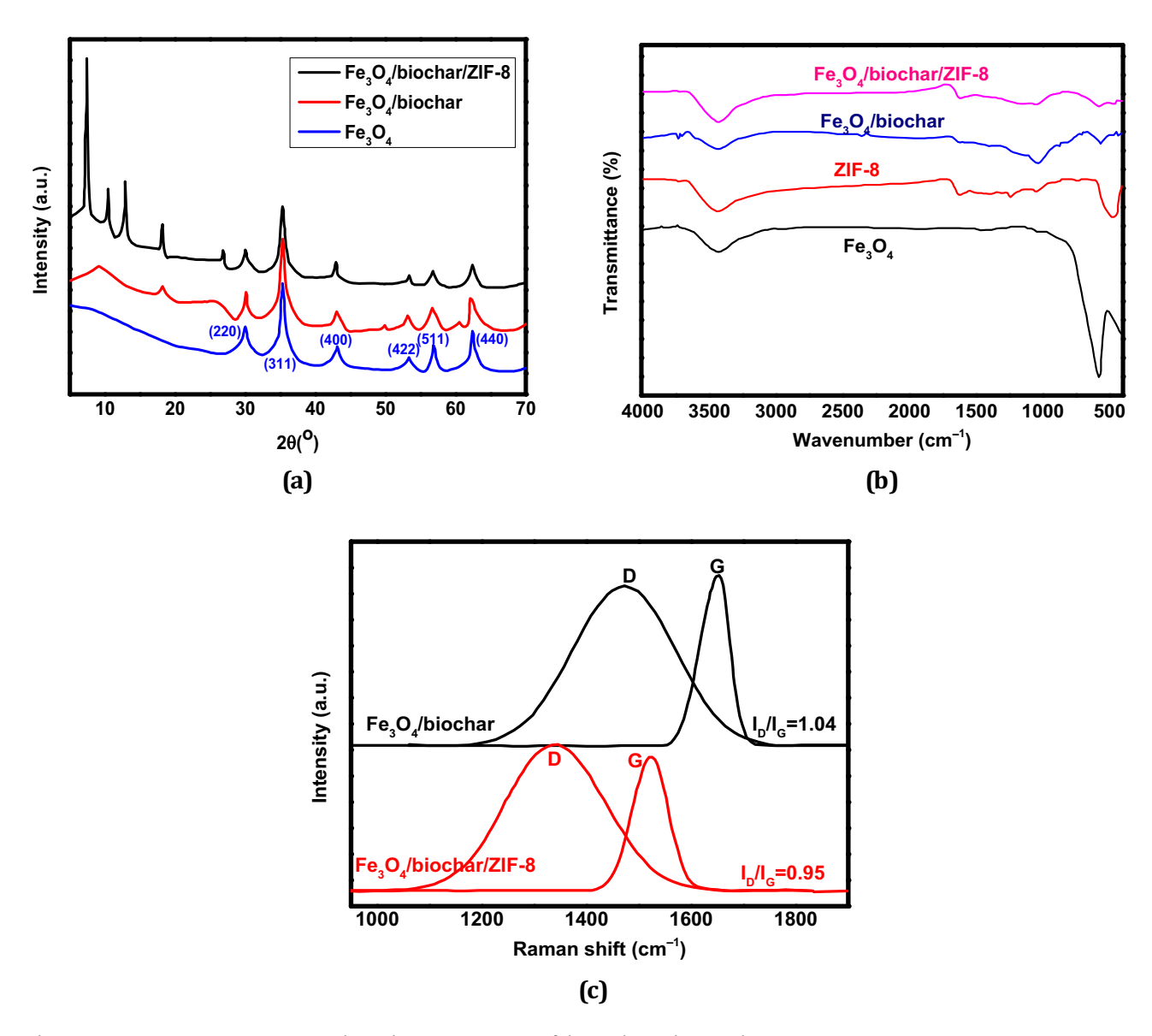


Figure 2: XRD patterns (a), FT-IR spectra (b), and Raman spectra (c) of the synthesized materials.

investigation of the $S_{\rm BET}$ surface area of synthesized materials [57] as shown in Figure 3b. According to Figure 3b, the synthesized biochar showed an $S_{\rm BET}$ of 8.97 m²·g⁻¹. The addition of magnetic nanoparticles to the biochar showed an increase in the $S_{\rm BET}$ to reach 280.55 m²·g⁻¹. Additionally, further addition of MOF ZIF-8 to the magnetic biochar increased the $S_{\rm BET}$ to reach 940.25 m²·g⁻¹. The $S_{\rm BET}$ of Fe₃O₄/biochar/ZIF-8 is about two times higher than that of Fe₃O₄/biochar. It appears that the addition of ZIF-8 facilitated the expansion of the surface area. The Fe₃O₄/biochar/ZIF-8 nanocomposite showed a combined feature of type I and IV phenomena, indicating the co-occurrence of micropores and mesopores that interpret the enhanced surface area. Additionally, the Fe₃O₄/biochar/ZIF-8 nanocomposite

shows an H4-type hysteresis loop at a relative pressure p/p^0 > 0.4, indicating the higher content of mesopores. In contrast, at a relative pressure p/p^0 < 0.01, the importance of micropores is very clear as the adsorption capacity was significantly increased. The mesoporous and microporous construction will aid in the improved migration of the adsorbate particles via the porous arrangement, increasing the capillary effect and improving the adsorption behavior of nanocomposites [58]. Therefore, the N_2 adsorption/desorption isotherms showed the significant effect of ZIF-8 MOF on the nanocomposite. The thermal stability of synthesized materials was determined using TGA analysis in the temperature range from 30 to 1,000°C, as shown in Figure 3c. According to the TGA curves of Fe₃O₄/biochar/ZIF-8 and

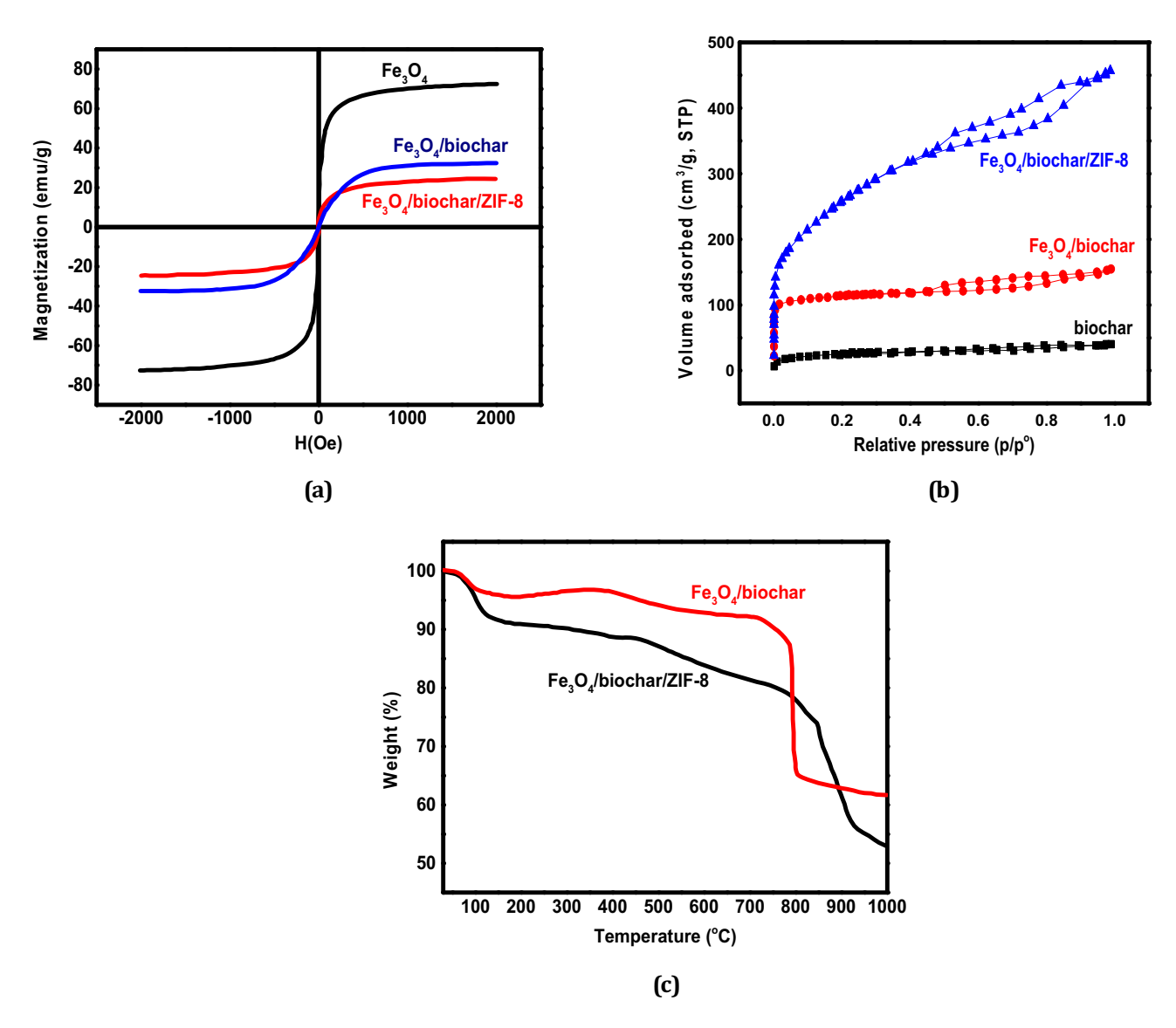


Figure 3: Magnetic hysteresis loops (a), the N₂ adsorption–desorption isotherms (b), and thermogravimetric analysis (TGA) (c) of the synthesized materials.

Fe₃O₄/biochar composites, the adsorbed surface water was evaporated in the temperature range from 30 to 100°C; however, the decomposition of functional groups in the composites was observed in the temperature range from 100 to 780°C. It is clear that the weight. loss of the Fe₃O₄/biochar/ZIF-8 nanocomposite was higher than that of the Fe₃O₄/biochar in the temperature range from 100 to 780°C by about 11%, which was attributed to the evaporation of the ZIF-8 MOF from the surface of the nanocomposite. The Fe₃O₄/biochar composite showed a rapid weight loss at 780°C, resulting from the decomposition of its carbon backbone. At a temperature higher than 900°C, the weight loss in the Fe₃O₄/biochar/ZIF-8 nanocomposite was attributed to the decomposition of the metallic Zn from the MOF. Therefore, the Fe₃O₄/biochar/ZIF-8 nanocomposite has a higher thermal stability than the

 Fe_3O_4 /biochar composite, which was attributed to the ZIF-8 MOF acting as a sacrificial template. All characterization results indicated the good fabrication of the nanocomposite Fe_3O_4 /biochar/ZIF-8.

3.2 Adsorption study

3.2.1 Adsorption isotherm and kinetics

To understand the adsorption behavior of Cr(vi) ions on the surface of the synthesized nanocomposites, the adsorption isotherm and kinetics were studied. Figure 4a shows the adsorption isotherms in which the initial concentration of Cr(vi) ions was varied with the adsorption capacities of the

8 — Norah Salem Alsaiari et al. DE GRUYTER

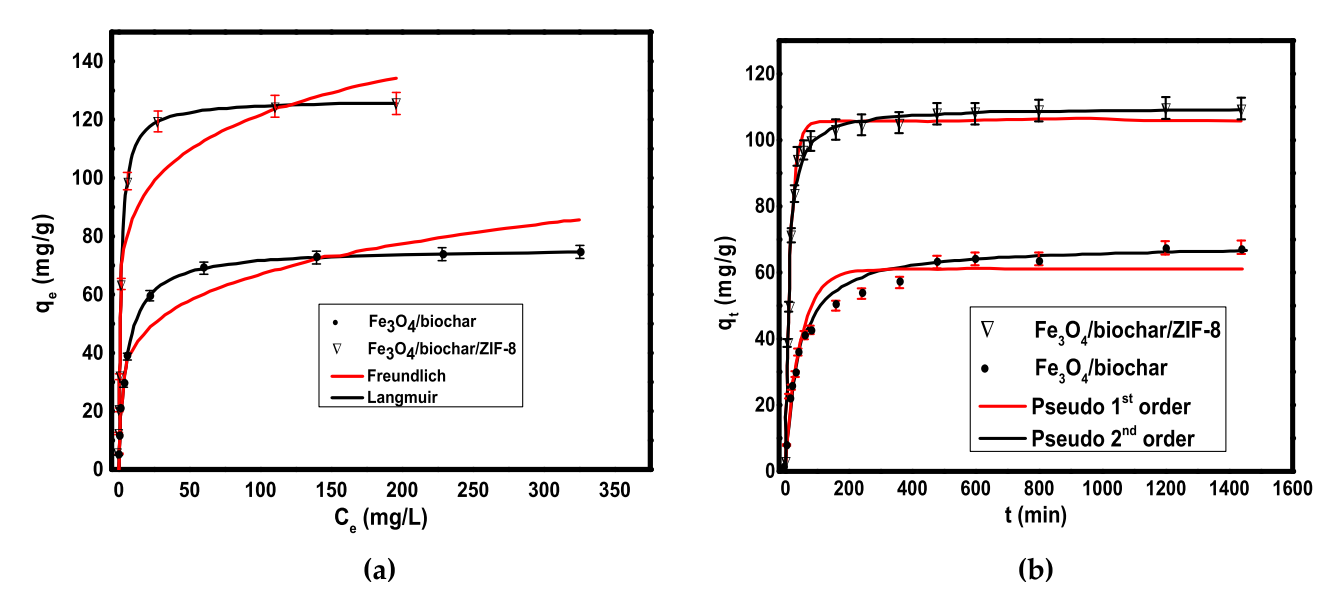


Figure 4: Adsorption isotherms models (a) and adsorption kinetics models (b) for the removal of $Cr(v_1)$ ions on the surface of the synthesized materials (initial concentration = 300 mg·L⁻¹, pH = 2, temperature = 25°C, adsorbent dose = 0.5 g, and contact time = 24 h).

prepared adsorbents. For both nanocomposites, Fe_3O_4 /biochar/ZIF-8 and Fe_3O_4 /biochar as adsorbents, the increase in the Cr(vi) initial concentration caused a rapid increase of the adsorption capacities until an equilibrium was reached at which the adsorption remains unchanged. Figure 4a shows the fitting of experimental adsorption data using the Freundlich equation – Eq. (1) – and Langmuir equation – Eq. (2) – for the better understanding of isotherms:

$$q_{\rm e} = K_{\rm F} C_{\rm e}^{1/2},$$
 (1)

$$q_{\rm e} = \frac{Q_{\rm max} K_{\rm L} C_{\rm e}}{1 + K_{\rm I} C_{\rm e}},\tag{2}$$

where $q_{\rm e}$ is the adsorption capacity (mg·g⁻¹) at equilibrium, $K_{\rm F}$ is the Freundlich equilibrium adsorption constant (mg¹⁻ⁿ·Lⁿ·g⁻¹), $K_{\rm L}$ is the Langmuir equilibrium adsorption constant (L·mg⁻¹), and $Q_{\rm max}$ is the maximum adsorption capacity (mg·g⁻¹). The Freundlich and Langmuir isotherm coefficients are presented in Table 1.

According to Figure 4a, the adsorption isotherms of Cr(vi) on the surface of both nanocomposites were better

defined using the Langmuir model than the Freundlich model, which is also from the R^2 values presented in Table 1. This indicated that the adsorption of metal on the surface of adsorbents occurred as a monolayer over the identical adsorption sites [59,60]. The coefficients presented in Table 1 indicate that the maximum adsorption capacities according to the Langmuir isotherm were 125 and 77 mg·g⁻¹ for Fe₃O₄/biochar/ZIF-8 and Fe₃O₄/biochar, respectively. The results of adsorption experiments show that even without ZIF-8 doping, the Fe₃O₄/biochar nanocomposite has a good adsorption capacity, which is attributed to the porous structure, large specific surface area, abundant mineral components, and surface functional groups. For comparison, Table 2 shows the maximum adsorption capacities of different MOF adsorbents in the Cr(vi) removal from water. The adsorption capacity of Fe₃O₄/biochar/ZIF-8 toward the removal of Cr(v_I) ions is higher than many previously prepared adsorbents. The adsorption of Cr(vI) ions on the surface of Fe₃O₄/biochar/ ZIF-8 and Fe₃O₄/biochar nanocomposites was favorable, as

Table 1: Adsorption isotherm and kinetic parameters for the adsorption of Cr(v1) ions on the surface of the synthesized materials

Adsorbent	ent Langmuir		Freundlich			Pseudo-first order			Pseudo-second order			
Parameters	q _m (mg·g ⁻¹)	<i>K</i> _L (L·mg ^{−1})	R ²	N	K _F (mg·g ⁻¹) (L·mg) ^{-1/n}	R ²	K ₁ (min ⁻¹)	q _e	R ²	<i>K</i> ₂ (g·mg.h ⁻¹)	q _e	R ²
Fe ₃ O ₄ /biochar	77.0	0.15	0.998	4.77	25.6	0.844	0.03	67.7	0.930	0.0005	68.7	0.997
Fe ₃ O ₄ /biochar/ ZIF-8	125.0	0.54	0.998	6.50	61.0	0.768	0.07	111.0	0.981	0.0010	111.0	0.999

Table 2: Comparison of the Fe_3O_4 /biochar/ZIF-8 nanocomposite with previously reported adsorbents for the adsorption of $Cr(v_I)$ ions

Adsorbent	рН	Removal capacity (mg·g ^{–1})	Reference		
Fe ₃ O ₄ /biochar/ZIF-8	2.0	125.0	This study		
Fe ₃ O ₄ @MIL-100	2.0	18.0	[67]		
MIL-100	2.0	30.4	[68]		
Amine-MIL-101	4.0	44.0	[69]		
Mn-UiO-66	_	32.77	[70]		
MOF BUC-17	4.0	121.0	[71]		
GO-CS@MOF	3.0	144.9	[72]		
ZIF-67	5.0	13.3	[73]		
ZIF-8	7.0	0.15	[74]		
Cu-BTC	7.0	40.0	[75]		

indicated by the separation factor ($R_{\rm L}$) values (from 0–1) [61,62]. Moreover, the stronger adsorption affinity of Fe₃O₄/biochar/ZIF-8 toward Cr(v_I) ions than Fe₃O₄/biochar was evident from the higher $R_{\rm L}$ values. This was because the introduction of the MOF (ZIF-8) to the nanocomposite provided more adsorption active sites. Additionally, the adsorption kinetics was investigated using pseudo-first- (Eq. (3)) and pseudo-second-order kinetics (Eq. (4)):

$$q_{\rm t} = q_{\rm e}(1 - e^{-k_{\rm l}t}),$$
 (3)

$$q_{\rm t} = \frac{k_2 q_{\rm e}^2 t}{1 + k_2 q_{\rm e} t},\tag{4}$$

where $q_{\rm t}$ (mg·g⁻¹) represents the adsorption capacity of the adsorbent at the reaction time t, $k_{\rm l}$ (min⁻¹) represents the rate constant of the pseudo-first-order kinetics, and $k_{\rm l}$ (g·mg⁻¹·min⁻¹) represents the rate constant of pseudo-second-order kinetics. The pseudo-first- and pseudo-second-order kinetic model coefficients are presented in Table 1.

The effect of time on the removal of Cr(vi) ions on the surface of Fe₃O₄/biochar/ZIF-8 and Fe₃O₄/biochar nanocomposites is shown in Figure 4b. Similar adsorption behavior was observed for both adsorbents. According to Figure 4b, the adsorption equilibrium for the removal of Cr(vi) ions on the surface of Fe₃O₄/biochar/ZIF-8 and Fe₃O₄/biochar nanocomposites was achieved at 300 and 500 min, respectively. Under high concentrations of Cr(vi) ions, it was a quick initial stage of adsorption aided by ion diffusion. After this stage, the rate of adsorption was decreased due to the saturation of adsorption sites with metal adsorbate ions. The effect of time indicated a faster adsorption of Cr(vI) ions on the Fe₃O₄/biochar/ZIF-8 than Fe₃O₄/biochar because the presence of a higher number of abundant functional groups facilitated the rapid uptake of ions. According to Table 1, the adsorption of Cr(vi) ions on

Fe₃O₄/biochar/ZIF-8 than the Fe₃O₄/biochar adsorbent was best described using a pseudo-second-order kinetic model as indicated by the correlation coefficient (R^2) values. This indicated that the adsorption of both adsorbents was achieved using chemical and physical methods [63]. In the physical method, the diffusion of ions was achieved within the pores of nanocomposites; whereas, in the chemical method, by complexation of ions was achieved by the functional groups and reduction. This kinetic behavior of Cr(vi) adsorption was observed with previously reported adsorbents [64–66].

3.2.2 Effect of competing ions and the ionic strength

To understand the efficiency of any adsorbent for the removal of contaminants, the effect of competing ions should be investigated to determine the selectivity of the adsorbent toward targeted ions. Therefore, the competition between $Cr(v_I)$ ions and competing ions for the adsorption active sites on the surface of $Fe_3O_4/biochar/ZIF-8$ and $Fe_3O_4/biochar$ was investigated, as shown in Figure 5a. According to Figure 5a, the adsorption of $Cr(v_I)$ ions on the surface of the $Fe_3O_4/biochar$ nanocomposite was slightly affected by the presence of Ca^{2+} , Fe^{3+} , and Cl^- ions, as well as slightly affected by the presence of PO_4^{3-} and SO_4^{2-} .

Also, the adsorption of Cr(vI) ions on the surface of Fe₃O₄/biochar/ZIF-8 was significantly affected by the competing ions and the effect was in the order $SO_4^{2-} > Fe^{3+} >$ $PO_4^{3-} > Ca^{2+} > Cl^-$. The SO_4^{2-} ions had a higher effect on the removal of Cr(vi) ions than PO₄³⁻ ions. This is attributed to the less net charge of PO₄³⁻ than Cr₂O₇²⁻ at pH 2, as it exists as HPO₄²⁻ and H₃PO₄ while SO₄²⁻ carries two negative charges, such as Cr₂O₇^{2-,} with the same molecular structure producing a higher competition for adsorption sites [76,77]. The complexation of Cr(vI) oxyanions with Fe³⁺ and Ca²⁺ ions was the reason for the high effect on the adsorption process [78]. Another important factor affecting the adsorption of Cr (vi) ions is the ionic strength, as shown in Figure 5b, in which the adsorption was studied on the surface of Fe₃O₄/biochar/ ZIF-8 and Fe₃O₄/biochar nanocomposites at different concentrations of NO₃⁻ ions. According to Figure 5b, the increase of NO₃ concentration caused a decrease in the adsorption efficiency of the Fe₃O₄/biochar/ZIF-8 nanocomposite. The increase of NO₃⁻ concentration to 0.1 mg·L⁻¹ caused a decrease in adsorption efficiency by 39%. However, for the Fe₃O₄/biochar nanocomposite, the reduction in the adsorption efficiency was only 11%. The main cause of the decreased Cr(vi) removal at an increased ionic strength was the competition between Cr(vi) and NO₃ ions for the adsorption sites [79].

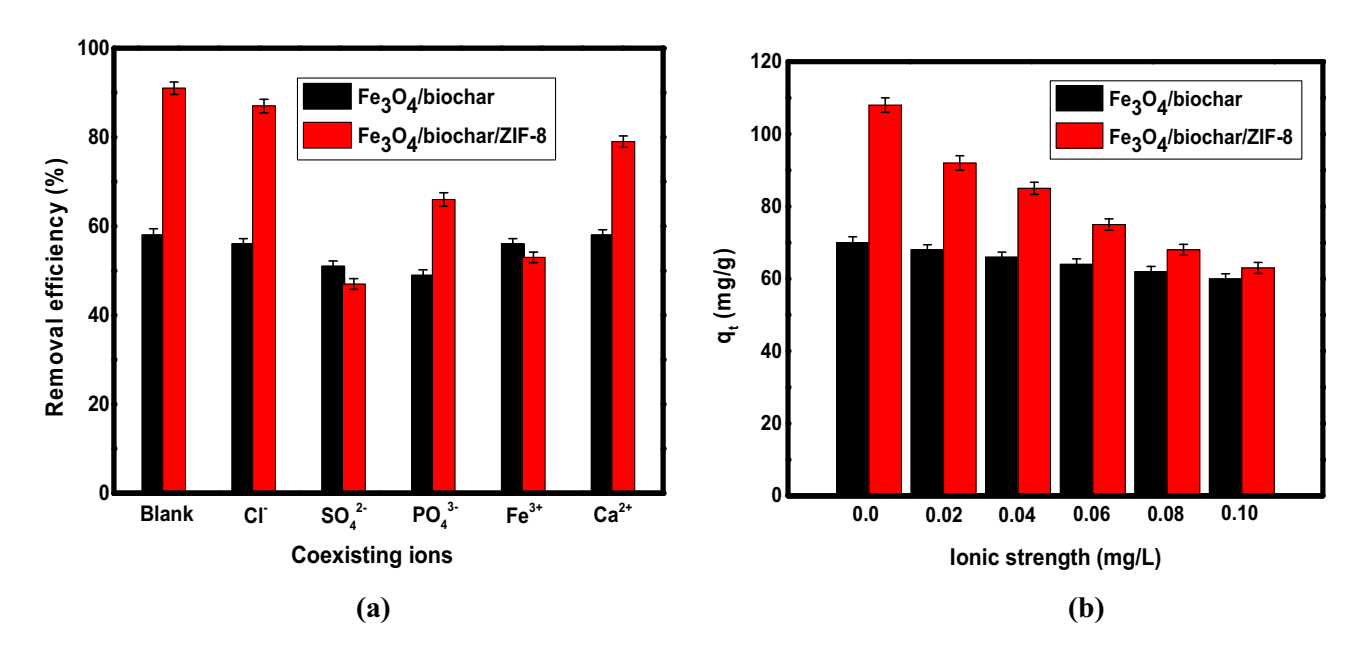


Figure 5: The effect of 0.01 M competing ions (a) and the effect of the ionic strength (b) on the adsorption of Cr(vI) ions on the surface of the synthesized materials.

3.2.3 Effect of pH values

It is well-known that one of the key elements that greatly affects the removal of $Cr(v_1)$ from aqueous solution is the pH value [80] because the solution pH also influences the charge of the adsorbent surface in addition to the species and redox potential of $Cr(v_1)$ that are already present [81,82]. Therefore, the effect of solution pH on the removal of $Cr(v_1)$ from aqueous solution on the surface of $Fe_3O_4/$

biochar/ZIF-8 and Fe₃O₄/biochar nanocomposites was investigated, as shown in Figure 6a.

While the adsorption behavior between Fe₃O₄/biochar/ZIF-8 and Fe₃O₄/biochar nanocomposites was different, the solution pH clearly had a great effect on the removal of Cr(vi) ions. According to Figure 6a, Fe₃O₄/biochar nanocomposites exhibited a limited pH range for the removal of Cr(vi) ions (pH = 1–4) while the Fe₃O₄/biochar/ZIF-8 nanocomposite exhibited a wide pH range (pH = 2–10) for the

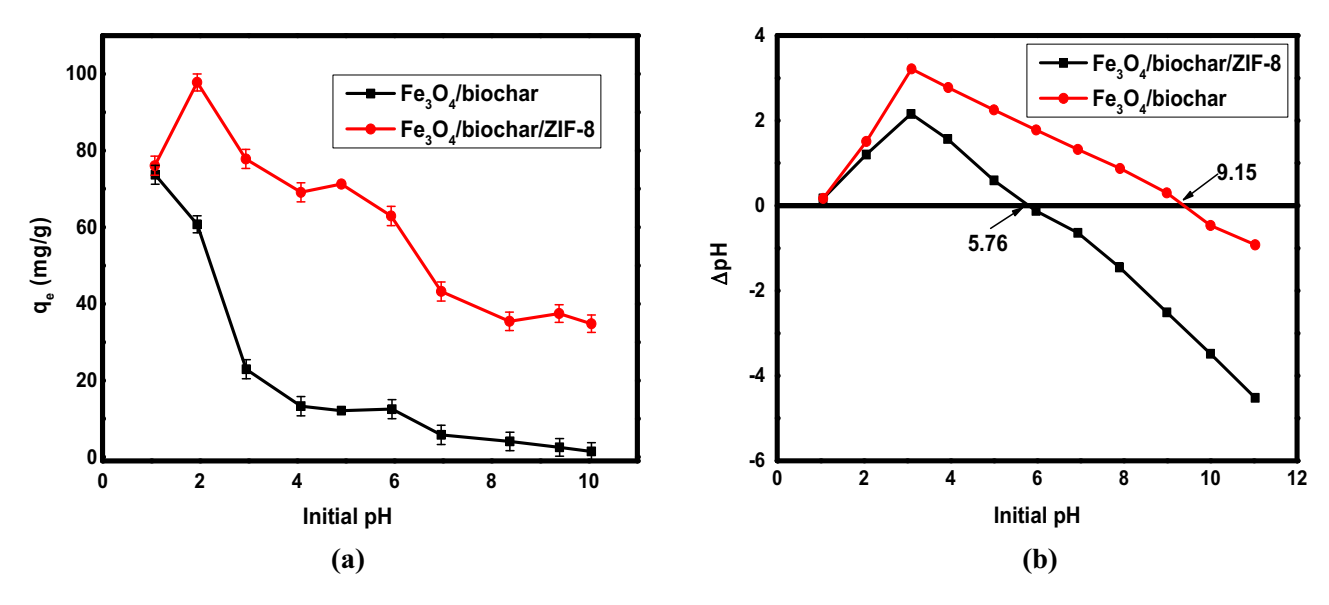


Figure 6: The effect of pH (a) and the point of zero charge (pH $_{Dzr}$) (b) for the adsorption of Cr(vi) ions on the surface of the synthesized materials.

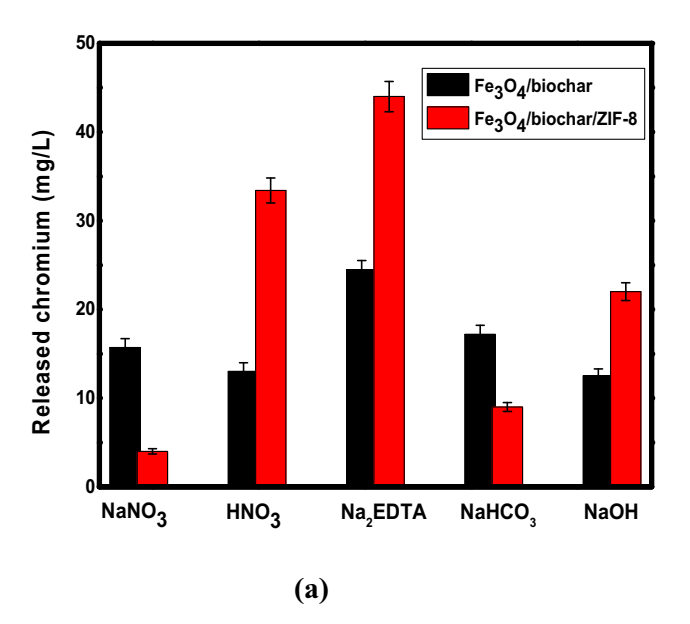
Cr(vi) adsorption. For the Fe₃O₄/biochar nanocomposite, the increased pH value from 1 to 3 caused an increased adsorption efficiency toward Cr(vI) ions, and this adsorption efficiency was decreased at pH 7. For the Fe₃O₄/biochar/ZIF-8 nanocomposite, the adsorption capacity was still high even after the pH increased up to 10, and higher than that of the Fe₃O₄/biochar nanocomposite by about 31%. However, the increased pH value also reduced the adsorption efficiency of the pollutant over both the adsorbents. To better understand the pH effect, the was investigated, as shown in Figure 6b. According to Figure 6b, the pH_{DZC} values were 9.15 and 5.76 for Fe₃O₄/biochar and Fe₃O₄/ biochar/ZIF-8, respectively. The higher value of Fe₃O₄/biochar/ ZIF-8 was attributed to the introduced MOF. After adsorption, pH variations in the solution were also noticed. The pH of the solution after adsorption on the surface of Fe₃O₄/biochar was a little lower than the pH_{pzc} value, thereby reducing its adsorption efficiency. Apart from the changes in the Cr(v1) percentage with the increasing solution pH, the electrostatic repulsion between the negatively charged Fe₃O₄/biochar/ZIF-8 surface and Cr(vi) anions was the primary cause of the decrease in the adsorption efficiency at pH > 6. Additionally, the higher adsorption efficiency of Fe₃O₄/biochar/ZIF-8 at low pH values than Fe₃O₄/biochar was attributed to the protonated functional groups on its surface. When the adsorption solution was analyzed after adsorption at low pH values, the presence of Cr(III) ions was approved, indicating the reduction of Cr(vi) ions. This reduction of Cr(vi) ions to Cr(iii) ions is well known with the biochar adsorbents due to their role as electron donors and electron acceptors as discussed in the literature [83,84].

Subsequently, the removal of Cr(vi) ions on the surfaces of Fe₃O₄/biochar/ZIF-8 and Fe₃O₄/biochar was achieved *via* different mechanisms.

3.2.4 Regeneration and reusability study

Regeneration and reusability study for any adsorbent is very important economically as it decreases the overall cost of the treatment process [85–87]. Before reusing the adsorbents, the desorption of adsorbed pollutants should be investigated first. Therefore, many eluents have been explored to desorb Cr(vi) ions from the surface of the synthesized $Fe_3O_4/biochar/ZIF-8$ and $Fe_3O_4/biochar$ as adsorbents, as shown in Figure 7a.

According to Figure 7a, the desorption efficiency toward Cr(vi) ions from the surface of Fe_3O_4 /biochar/ZIF-8 was in the order of $NaNO_3$ < $NaHCO_3$ < NaOH < HNO_3 < Na_2EDTA , whereas for Fe_3O_4 /biochar, the desorption efficiency toward Cr(vi) ions was in the order of NaOH < HNO_3 < $NaNO_3$ < $NaHCO_3$ < Na_2EDTA , as shown in Figure 7a. It is clear that the sodium EDTA salt has the highest desorption capacity toward Cr(vi) ions. The acids HCl and HNO_3 showed good desorption capacities toward Cr(vi) ions from the surface of Fe_3O_4 /biochar/ZIF-8 and Fe_3O_4 /biochar, which was similar to the literature [88,89]. However, the commonly used desorption eluent for Cr(vi) ions is the basic solution of NaOH [90,91]. According to the desorption experimental results, the Na_2EDTA solution was used as an eluent to desorb Cr(vi) ions from the surface of Fe_3O_4 /biochar/ZIF-8 and Fe_3O_4 /biochar during the



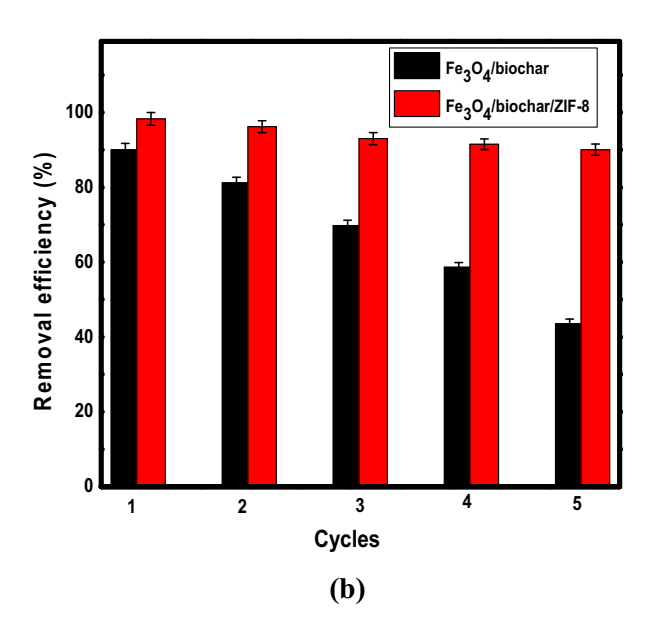


Figure 7: The desorption of total Cr ions using different eluents (a) and the reusability study (b) for the adsorption of Cr(vi) ions on the surface of the synthesized materials.

reusability study. The reusability of Fe₃O₄/biochar/ZIF-8 and Fe₃O₄/biochar for the removal of Cr(v₁) ions was investigated for five successive adsorption—desorption cycles as shown in Figure 7b. According to Figure 7b, the Fe₃O₄/biochar/ZIF-8 showed higher reusability results than Fe₃O₄/biochar. For both adsorbents, the removal efficiency was the highest in the first cycle due to the availability of vacant adsorption sites. After that, the removal efficiency was decreased cycle by cycle until it reached its minimum in the fifth cycle due to the destroyed adsorption sites resulting after each cycle. The removal efficiency of Fe₃O₄/biochar/ZIF-8 toward Cr(v₁) removal remained higher than 90.0% even after the last cycle, whereas for Fe₃O₄/biochar, the removal efficiency was decreased gradually from 90.5 to 45% in the last cycle.

The reusability results indicated that $Fe_3O_4/biochar/ZIF-8$ is a promising adsorbent to eliminate pollutants from water with cost-effective properties.

3.2.5 Suggested mechanism of adsorption

To study the mechanism of adsorption of Cr(vi) ions on the surface of Fe₃O₄/biochar/ZIF-8, XPS spectra of Fe₃O₄/biochar/ZIF-8 before and after adsorption were recorded, as shown in Figure 8a and b, respectively, to provide information regarding the surface chemistry of the adsorbent. Comparing Figure 8a and b showed a change in the metal (Zn) binding energy after and before adsorption, indicating

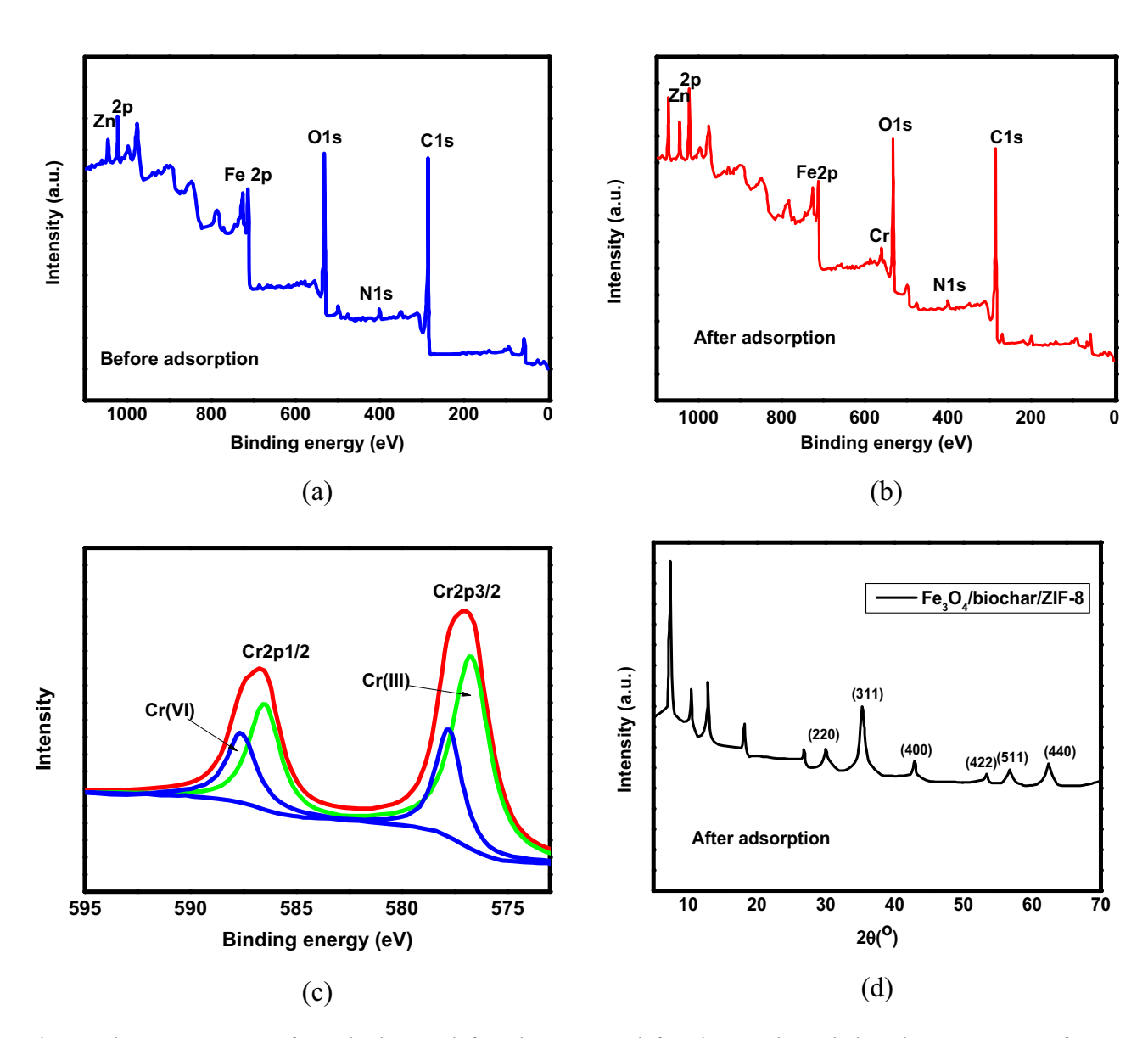


Figure 8: The XPS survey spectra of Fe_3O_4 /biochar/ZIF-8 before adsorption (a) and after adsorption (b). XPS high-resolution Cr 2p spectra of Fe_3O_4 /biochar/ZIF-8 after the removal of Cr(vI) ions (c), and XRD patterns of Fe_3O_4 /biochar/ZIF-8 after adsorption (d).

that metal sites were involved in the chelation process. Also, the XPS spectra after adsorption showed the appearance of a new binding energy peak at 580 eV, which belongs to Cr(vi) ions, confirming their presence on the surface of the adsorbent. Additionally, the identification of the adsorbed species of chromium ions was achieved using high-resolution XPS spectra as shown in Figure 8c. According to Figure 8c, the high-resolution XPS spectra showed the presence of two satellite bands of Cr(III) and Cr(vi) ions at 587 and 577 eV, respectively. Subsequently, the presence of two chromium species Cr(III) and Cr(VI) on the surface of Fe₃O₄/biochar/ZIF-8 indicated the removal of Cr(vi) ions on the adsorbent surface by adsorption and by the chemical reduction to Cr(III). In this regard, the mechanism of Cr(vi) removal can be explained as follows: the protonated nitrogen and oxygen functional groups on the surface of adsorbent under acidic conditions can adsorb Cr(v_I) species (HCrO₄⁻) via electrostatic interactions and chemical bonding. This chemical bonding on the surface of adsorbent was also associated with the chemical reduction of Cr(vi) to Cr(iii). The chemical bonding also occurred through the metal sites (Zn) of the MOFs. The resulting Cr(III) ions could be removed by complexation with functional groups on the adsorbent surface and others may be dissolved in water.

The study of adsorbent stability is very important. Therefore, the stability of Fe₃O₄/biochar/ZIF-8 as an adsorbent was determined by XRD after adsorption, as shown in Figure 8d. According to Figure 8d and comparing with the results of XRD before adsorption, there is no change in the XRD patterns before and after adsorption. These results indicate the good stability of Fe₃O₄/biochar/ZIF-8 as an adsorbent. To confirm this stability of Fe₃O₄/biochar/ZIF-8 as an adsorbent, the concentration of Fe and C in the solution after equilibrium was measured. Carbon was found to be 0.51-0.71% and Fe was found to be 0.2-0.3% under acidic conditions. These results also confirmed the high stability of Fe₃O₄/biochar/ZIF-8 and the gained stability by MOF modification.

The present MOF-based adsorbent has several advantages such as excellent designability with the control of pore size, pore type, adsorption sites, and surface area that affect the adsorption capacity. This MOF-based adsorbent with a controlled chemical design and pore structure allows its application in water treatment. Another advantage is the reusability with high adsorption efficiency, which reduces the overall cost of treatment so it is costeffective. Also, it is very stable and easily collected from the reaction medium due to its magnetic properties. It can capture pollutants with different mechanisms due to the diversity of functional groups on its surface. It is very selective and can be used in the presence of competing ions and at a wide pH range. However, like any adsorbent material, it has some disadvantages such as the difficulty of connecting the MOFs with the matrix, high cost of synthesis, long time synthesis, and high accuracy and skill during the synthesis.

4 Conclusions

In summary, Fe₃O₄/biocha, and Fe₃O₄/biochar/ZIF-8 nanocomposites were synthesized by the one-pot hydrothermal method. The citrus fruits as a source of biochar were mixed with magnetic nanoparticles and MOFs to synthesize a novel nanocomposite of Fe₃O₄/biochar/ZIF-8. The nanocomposite was well characterized using different techniques including SEM, XRD, FT-IR, Raman spectroscopy, the N₂ adsorption-desorption isotherm, TGA, and magnetization curves. All these results showed an excellent combination between the three components of the nanocomposite. The nanocomposite was employed as a recyclable ecological adsorbent for the effective removal of Cr(vi) ions from the aqueous solution. The Fe₃O₄/biochar/ZIF-8 nanocomposite showed improved adsorption capacities toward the examined pollutant. The adsorption data were well-described using the Langmuir isotherm model and pseudo-second-order kinetic model, indicating monolayer and physicochemical adsorption. The adsorption capacities were found to be 77 and 125 mg·g⁻¹ for Fe₃O₄/biochar and Fe₃O₄/biochar/ZIF-8, respectively, according to the Langmuir model. The results indicated the role of MOFs as a matrix that holds the nanoparticles and improves their properties. The effect of different parameters on adsorption has been investigated, including pH, ionic strength, and competing ions. The results showed that the studied material has a good adsorption capacity at different ionic strength values and in the presence of different competing ions, indicating its applicability in real water treatment. Moreover, the Fe₃O₄/biochar/ZIF-8 nanocomposite showed excellent reusability toward Cr(vi) removal. The removal mechanism of Cr(vI) ions on the surface of the nanocomposite was studied and the results indicated the removal of ions by chemical bonding with the zinc metal, nitrogen, and oxygen centers, chemical reduction of Cr(vI) ions to Cr(III) ions, and electrostatic interaction. The XRD results of the nanocomposite after adsorption showed its good stability as an adsorbent. We can conclude that the Fe₃O₄/biochar/ZIF-8 nanocomposite is a promising recyclable adsorbent for the removal of pollutants from water.

Acknowledgments: The authors extend their appreciation to the Deanship of Scientific Research at King Khalid University for funding this work through the research groups program (grant no. RGP.2/34/44). This research was also funded by the Princess Nourah bint Abdulrahman University Researchers Supporting Project (number PNURSP2023R19), Princess Nourah bint Abdulrahman University, Riyadh, Saudi Arabia.

Funding information: This research was funded by the Deanship of Scientific Research at King Khalid University (grant no. RGP.2/34/44). Additionally, this research was funded by the Princess Nourah bint Abdulrahman University Researchers Supporting Project (number PNURSP2023R19), Princess Nourah bint Abdulrahman University, Riyadh, Saudi Arabia.

Author contributions: Conceptualization, N.S.A. and F.M.A.; methodology, K.M.K.; software, M.S.A.; validation, F.M.A., K.M.K. and M.S.A.; formal analysis, F.M.A.; investigation, K.M.K.; resources, K.M.K.; data curation, F.M.A.; writing – original draft preparation, F.M.A.; writing – review and editing, K.M.K.; visualization, A.A.; supervision, M.A.T.; project administration, A.A.; funding acquisition, N.S.A. All authors have accepted responsibility for the entire content of this manuscript and approved its submission.

Conflict of interest: The authors state no conflict of interest.

Data availability statement: The datasets generated and/ or analyzed during the current study are available from the corresponding author upon reasonable request.

References

- [1] Cherdchoo, W., S. Nithettham, and J. Charoenpanich. Removal of Cr (VI) from synthetic wastewater by adsorption onto coffee ground and mixed waste tea. *Chemosphere*, Vol. 221, 2019, pp. 758–767.
- [2] Niu, J., P. Ding, X. Jia, G. Hu, and Z. Li. Study of the properties and mechanism of deep reduction and efficient adsorption of Cr (VI) by low-cost Fe3O4-modified ceramsite. Science of the Total Environment, Vol. 688, 2019, pp. 994–1004.
- [3] Han, S., Y. Zang, Y. Gao, Q. Yue, P. Zhang, W. Kong, et al. Commonomer polymer anion exchange resin for removing Cr (VI) contaminants: Adsorption kinetics, mechanism and performance. Science of The Total Environment, Vol. 709, 2020, id. 136002.
- [4] Coetzee, J. J., N. Bansal, and E. M. Chirwa. Chromium in environment, its toxic effect from chromite-mining and ferrochrome industries, and its possible bioremediation. *Exposure and Health*, Vol. 12, 2020, pp. 51–62.
- [5] Mortada, W. I., A. El-Naggar, A. Mosa, K. N. Palansooriya, B. Yousaf, R. Tang, et al. Biogeochemical behaviour and toxicology of chromium in the soil-water-human nexus: A review. *Chemosphere*, Vol. 331, 2023, id. 138804.

- [6] Mahmoud, M. E., S. M. Elsayed, S. E. M. Mahmoud, R. O. Aljedaani, and M. A. Salam. Recent advances in adsorptive removal and catalytic reduction of hexavalent chromium by metal–organic frameworks composites. *Journal of Molecular Liquids*, Vol. 347, 2022, id. 118274.
- [7] Xie, Y., J. Lin, J. Liang, M. Li, Y. Fu, and H. Wang. Hypercrosslinked mesoporous poly (ionic liquid) s with high density of ion pairs: Efficient adsorbents for Cr (VI) removal via ion-exchange. *Chemical Engineering Journal*, Vol. 378, 2019, id. 122107.
- [8] Tavakoli, O., V. Goodarzi, M. R. Saeb, N. M. Mahmoodi, and R. Borja. Competitive removal of heavy metal ions from squid oil under isothermal condition by CR11 chelate ion exchanger. *Journal of Hazardous Materials*, Vol. 334, 2017, pp. 256–266.
- [9] He, P. Y., Y. J. Zhang, H. Chen, Z. C. Han, and L. C. Liu. Low-cost and facile synthesis of geopolymer-zeolite composite membrane for chromium (VI) separation from aqueous solution. *Journal of Hazardous Materials*, Vol. 392, 2020, id. 122359.
- [10] Masinire, F., D. O. Adenuga, S. M. Tichapondwa, and E. M. Chirwa. Phytoremediation of Cr (VI) in wastewater using the vetiver grass (Chrysopogon zizanioides). *Minerals Engineering*, Vol. 172, 2021, id. 107141.
- [11] Banerjee, S, B. Kamila, S. Barman, S. R. Joshi, T. Mandal, G. Halder. Interlining Cr (VI) remediation mechanism by a novel bacterium Pseudomonas brenneri isolated from coalmine wastewater. *Journal of Environmental Management*, Vol. 233, 2019, pp. 271–282.
- [12] Yao, F., M. Jia, Q. Yang, K. Luo, F. Chen, Y. Zhong, et al. Electrochemical Cr (VI) removal from aqueous media using titanium as anode: Simultaneous indirect electrochemical reduction of Cr (VI) and in-situ precipitation of Cr (III). *Chemosphere*, Vol. 260, 2020, id. 127537.
- [13] Damiri, F., S. Andra, N. Kommineni, S. K. Balu, R. Bulusu, A. A. Boseila, et al. Recent advances in adsorptive nanocomposite membranes for heavy metals ion removal from contaminated water: A comprehensive review. *Materials*, Vol. 15, 2022, id. 5392.
- [14] Mpouras, T., A. Polydera, D. Dermatas, N. Verdone, and G. Vilardi. Multi wall carbon nanotubes application for treatment of Cr (VI)contaminated groundwater; Modeling of batch & column experiments. *Chemosphere*, Vol. 269, 2021, id. 128749.
- [15] Mousavi, S. R., M. Asghari, and N. M. Mahmoodi. Chitosan-wrapped multiwalled carbon nanotube as filler within PEBA thin film nanocomposite (TFN) membrane to improve dye removal. *Carbohydrate Polymers*, Vol. 237, 2020. id. 116128.
- [16] Tu, B., R. Wen, K. Wang, Y. Cheng, Y. Deng, W. Cao, et al. Efficient removal of aqueous hexavalent chromium by activated carbon derived from Bermuda grass. *Journal of Colloid and Interface Science*, Vol. 560, 2020, pp. 649–658.
- [17] Cheng, Q., C. Wang, K. Doudrick, and C. K. Chan. Hexavalent chromium removal using metal oxide photocatalysts. *Applied Catalysis B: Environmental*, Vol. 176, 2015, pp. 740–748.
- [18] Mahmoodi, N. M., M. Ghezelbash, M. Shabanian, F. Aryanasab, and M. R. Saeb. Efficient removal of cationic dyes from colored wastewaters by dithiocarbamate-functionalized graphene oxide nanosheets: From synthesis to detailed kinetics studies. *Journal of the Taiwan Institute of Chemical Engineers*, Vol. 81, 2017, pp. 239–246.
- [19] Ashour, E. A. and M. A. Tony. Eco-friendly removal of hexavalent chromium from aqueous solution using natural clay mineral: activation and modification effects. SN Applied Sciences, Vol. 2, 2020, pp. 1–13.
- [20] Geng, Z., Y. Lin, X. Yu, Q. Shen, L. Ma, Z. Li, et al. Highly efficient dye adsorption and removal: a functional hybrid of reduced graphene

- oxide-Fe₃O₄ nanoparticles as an easily regenerative adsorbent. Journal of Materials Chemistry, Vol. 22, 2012, pp. 3527-3535.
- [21] Zhu, L., D. Shen, C. Xu, X. Dai, M. A. Silver, J. Li, et al. Identifying the recognition site for selective trapping of 99TcO4-in a hydrolytically stable and radiation resistant cationic metal-organic framework. Journal of the American Chemical Society, Vol. 139, 2017, pp. 14873-14876.
- [22] Wang, Q., Q. Gao, A. M. Al-Enizi, A. Nafady, and S. Ma. Recent advances in MOF-based photocatalysis: environmental remediation under visible light. Inorganic Chemistry Frontiers, Vol. 7, 2020,
- [23] Goetjen, T. A., J. Liu, Y. Wu, J. Sui, X. Zhang, J. T. Hupp, et al. Metal-organic framework (MOF) materials as polymerization catalvsts: a review and recent advances. Chemical Communications. Vol. 56, 2020, pp. 10409-10418.
- [24] Ajdari, F. B., E. Kowsari, M. N. Shahrak, A. Ehsani, Z. Kiaei, H. Torkzaban, et al. A review on the field patents and recent developments over the application of metal organic frameworks (MOFs) in supercapacitors. Coordination Chemistry Reviews, Vol. 422, 2020, id. 213441.
- [25] Koo, W.-T., J.-S. Jang, and I.-D. Kim. Metal-organic frameworks for chemiresistive sensors. Chem, Vol. 5, 2019, pp. 1938-1963.
- [26] Ren, J., Y. Huang, H. Zhu, B. Zhang, H. Zhu, S. Shen, et al. Recent progress on MOF-derived carbon materials for energy storage. Carbon Energy, Vol. 2, 2020, pp. 176-202.
- [27] Chen, B., Y. Li, M. Li, M. Cui, W. Xu, L. Li, et al. Rapid adsorption of tetracycline in agueous solution by using MOF-525/graphene oxide composite. Microporous and Mesoporous Materials, Vol. 328, 2021, id. 111457.
- [28] Alsaiari, N. S., H. Osman, A. Amari, and M. A. Tahoon. The synthesis of metal-organic-framework-based ternary nanocomposite for the adsorption of organic dyes from aqueous solutions. Magnetochemistry, Vol. 8, 2022, id. 133.
- [29] Alzahrani, F. M., N. S. Alsaiari, K. M. Katubi, A. Amari, and M. A. Tahoon. Synthesis, characterization, and application of magnetized lanthanum (III)-based metal-organic framework for the organic dye removal from water. Adsorption Science & Technology, Vol. 2022,
- [30] Amari, A., F. M. Alzahrani, N. S. Alsaiari, K. M. Katubi, F. B. Rebah, and M. A. Tahoon. Magnetic metal organic framework immobilized laccase for wastewater decolorization. Processes, Vol. 9, 2021, id. 774.
- [31] Li, K., N. Miwornunyuie, L. Chen, H. Jingyu, P. S. Amaniampong, D. Ato Koomson, et al. Sustainable application of ZIF-8 for heavymetal removal in aqueous solutions. Sustainability, Vol. 13, 2021, id. 984.
- [32] Yu, F., X. Bai, M. Liang, and J. Ma. Recent progress on metal-organic framework-derived porous carbon and its composite for pollutant adsorption from liquid phase. Chemical Engineering Journal, Vol. 405, 2021, id. 126960.
- [33] Wu, Y., B. Li, X. Wang, S. Yu, H. Pang, Y. Liu, et al. Magnetic metalorganic frameworks (Fe3O4@ ZIF-8) composites for U (VI) and Eu (III) elimination: simultaneously achieve favorable stability and functionality. Chemical Engineering Journal, Vol. 378, 2019, id. 122105.
- [34] de Almeida, L. S., E. Q. Oreste, J. V. Maciel, M. G. Heinemann, and D. Dias. Electrochemical devices obtained from biochar: advances in renewable and environmentally-friendly technologies applied to analytical chemistry. Trends in Environmental. Analytical Chemistry, Vol. 26, 2020, id. e00089.

- [35] Zhou, Y., S. Qin, S. Verma, T. Sar, S. Sarsaiya, B. Ravindran, et al. Production and beneficial impact of biochar for environmental application: A comprehensive review. Bioresource Technology, Vol. 337, 2021, id. 125451.
- [36] Zhang, A., X. Li, J. Xing, and G. Xu. Adsorption of potentially toxic elements in water by modified biochar: A review. Journal of Environmental Chemical Engineering, Vol. 8, 2020, id. 104196.
- [37] Xiang, W., X. Zhang, J. Chen, W. Zou, F. He, X. Hu, et al. Biochar technology in wastewater treatment: A critical review. Chemosphere, Vol. 252, 2020, id. 126539.
- [38] Oladipo, A. A., E. O. Ahaka, and M. Gazi. High adsorptive potential of calcined magnetic biochar derived from banana peels for Cu²⁺, Hg²⁺, and Zn²⁺ ions removal in single and ternary systems. Environmental Science and Pollution Research, Vol. 26, 2019, pp. 31887-31899.
- [39] Dai, L., W. Zhu, L. He, F. Tan, N. Zhu, Q. Zhou, et al. Calcium-rich biochar from crab shell: an unexpected super adsorbent for dye removal. Bioresource Technology, Vol. 267, 2018, pp. 510-516.
- Ahmed, M., M. A. Islam, M. Asif, and B. Hameed. Human hairderived high surface area porous carbon material for the adsorption isotherm and kinetics of tetracycline antibiotics. Bioresource Technology, Vol. 243, 2017, pp. 778-784.
- Islam, M. A., M. Ahmed, W. Khanday, M. Asif, and B. Hameed. [41] Mesoporous activated coconut shell-derived hydrochar prepared via hydrothermal carbonization-NaOH activation for methylene blue adsorption. Journal of Environmental Management, Vol. 203, 2017, pp. 237-244.
- [42] Li, R., J. J. Wang, B. Zhou, M. K. Awasthi, A. Ali, Z. Zhang, et al. Recovery of phosphate from aqueous solution by magnesium oxide decorated magnetic biochar and its potential as phosphatebased fertilizer substitute. Bioresource Technology, Vol. 215, 2016,
- [43] Zhou, Y., S. Cao, C. Xi, X. Li, L. Zhang, G. Wang, et al. A novel Fe3O4/graphene oxide/citrus peel-derived bio-char based nanocomposite with enhanced adsorption affinity and sensitivity of ciprofloxacin and sparfloxacin. Bioresource Technology, Vol. 292, 2019, id. 121951.
- Han, Y., X. Cao, X. Ouyang, S. P. Sohi, and J. Chen. Adsorption kinetics of magnetic biochar derived from peanut hull on removal of Cr (VI) from aqueous solution: effects of production conditions and particle size. Chemosphere, Vol. 145, 2016, pp. 336-341.
- [45] Thines, K., E. Abdullah, N. Mubarak, and M. Ruthiraan. Synthesis of magnetic biochar from agricultural waste biomass to enhancing route for waste water and polymer application: a review. Renewable and Sustainable Energy Reviews, Vol. 67, 2017, pp. 257-276.
- [46] Zhou, Y., G. Liu, J. Liu, Y. Xiao, T. Wang, and Y. Xue. Magnetic biochar prepared by electromagnetic induction pyrolysis of cellulose: Biochar characterization, mechanism of magnetization and adsorption removal of chromium (VI) from aqueous solution. Bioresource Technology, Vol. 337, 2021, id. 125429.
- Liu, Q., B. Zhou, M. Xu, and G. Mao. Integration of nanosized ZIF-8 [47] particles onto mesoporous TiO 2 nanobeads for enhanced photocatalytic activity. RSC Advances, Vol. 7, 2017, pp. 8004-8010.
- Chen, J.-Y., S.-R. Cao, C.-X. Xi, Y. Chen, X.-L. Li, L. Zhang, et al. A novel magnetic β-cyclodextrin modified graphene oxide adsorbent with high recognition capability for 5 plant growth regulators. Food Chemistry, Vol. 239, 2018, pp. 911-919.
- [49] Deng, H., X. Li, Q. Peng, X. Wang, J. Chen and Y. Li. Monodisperse magnetic single-crystal ferrite microspheres. Angewandte Chemie International Edition, Vol. 44, 2005, pp. 2782-2785.

- [50] Tran, H. N., F. Tomul, N. T. H. Ha, D. T. Nguyen, E. C. Lima, G. T. Le, et al. Innovative spherical biochar for pharmaceutical removal from water: Insight into adsorption mechanism. *Journal of Hazardous Materials*, Vol. 394, 2020, id. 122255.
- [51] Liang, C., Y. Tang, X. Zhang, H. Chai, Y. Huang, and P. Feng. ZIF-mediated N-doped hollow porous carbon as a high performance adsorbent for tetracycline removal from water with wide pH range. Environmental Research. Vol. 182, 2020. jd. 109059.
- [52] Zhang, Y., T. Zhang, C. Guo, J. Lv, Z. Hua, S. Hou, et al. Drugs of abuse and their metabolites in the urban rivers of Beijing, China: occurrence, distribution, and potential environmental risk. *Science* of the Total Environment, Vol. 579, 2017, pp. 305–313.
- [53] Li, K., P. Du, Z. Xu, T. Gao, and X. Li. Occurrence of illicit drugs in surface waters in China. *Environmental Pollution*, Vol. 213, 2016, pp. 395–402.
- [54] Bedin, K. C., A. L. Cazetta, I. P. Souza, O. Pezoti, L. S. Souza, P. S. Souza, et al. Porosity enhancement of spherical activated carbon: Influence and optimization of hydrothermal synthesis conditions using response surface methodology. *Journal of Environmental Chemical Engineering*, Vol. 6, 2018, pp. 991–999.
- [55] Feng, D., Y. Zhao, Y. Zhang, S. Sun, S. Meng, Y. Guo, et al. Effects of K and Ca on reforming of model tar compounds with pyrolysis biochars under H₂O or CO₂. Chemical Engineering Journal, Vol. 306, 2016, pp. 422–432.
- [56] Sui, Z.-Y., X. Li, Z.-Y. Sun, H.-C. Tao, P.-Y. Zhang, L. Zhao, et al. Nitrogen-doped and nanostructured carbons with high surface area for enhanced oxygen reduction reaction. *Carbon*, Vol. 126, 2018, pp. 111–118.
- [57] Zhu, L., N. Zhao, L. Tong, Y. Lv, and G. Li. Characterization and evaluation of surface modified materials based on porous biochar and its adsorption properties for 2, 4-dichlorophenoxyacetic acid. *Chemosphere*, Vol. 210, 2018, pp. 734–744.
- [58] Cazetta, A. L., O. Pezoti, K. C. Bedin, T. L. Silva, A. Paesano Junior, T. Asefa, et al. Magnetic activated carbon derived from biomass waste by concurrent synthesis: efficient adsorbent for toxic dyes. ACS Sustainable Chemistry & Engineering, Vol. 4, 2016, pp. 1058–1068.
- [59] Zhang, Z., H. Li, J. Li, X. Li, Z. Wang, X. Liu, et al. A novel adsorbent of core-shell construction of chitosan-cellulose magnetic carbon foam: synthesis, characterization and application to remove copper in wastewater. *Chemical Physics Letters*, Vol. 731, 2019, id. 136573.
- [60] Kong, D., L. He, H. Li, and Z. Song. Preparation and characterization of graphene oxide/chitosan composite aerogel with high adsorption performance for Cr (VI) by a new crosslinking route. *Colloids* and Surfaces A: Physicochemical and Engineering Aspects, Vol. 625, 2021, id. 126832.
- [61] Gupta, S. and A. Kumar. Removal of nickel (II) from aqueous solution by biosorption on A. barbadensis Miller waste leaves powder. Applied Water. *Science*, Vol. 9, 2019, pp. 1–11.
- [62] Zhao, P., N. Liu, C. Jin, H. Chen, Z. Zhang, L. Zhao, et al. UiO-66: an advanced platform for investigating the influence of functionalization in the adsorption removal of pharmaceutical waste. *Inorganic Chemistry*, Vol. 58, 2019, pp. 8787–8792.
- [63] Han, Q., J. Wang, B. A. Goodman, J. Xie, and Z. Liu. High adsorption of methylene blue by activated carbon prepared from phosphoric acid treated eucalyptus residue. *Powder Technology*, Vol. 366, 2020, pp. 239–248.
- [64] Liu, H., F. Zhang, and Z. Peng. Adsorption mechanism of Cr (VI) onto GO/PAMAMs composites. *Scientific Reports*, Vol. 9, 2019, id. 3663.

- [65] Mei, J., H. Zhang, Z. Li, and H. Ou. A novel tetraethylenepentamine crosslinked chitosan oligosaccharide hydrogel for total adsorption of Cr (VI). *Carbohydrate Polymers*, Vol. 224, 2019, id. 115154.
- [66] Niu, C., N. Zhang, C. Hu, C. Zhang, H. Zhang, and Y. Xing. Preparation of a novel citric acid-crosslinked Zn-MOF/chitosan composite and application in adsorption of chromium (VI) and methyl orange from aqueous solution. *Carbohydrate Polymers*, Vol. 258, 2021, id. 117644.
- [67] Yang, Q., Q. Zhao, S. Ren, Q. Lu, X. Guo, and Z. Chen. Fabrication of core-shell Fe₃O₄@ MIL-100 (Fe) magnetic microspheres for the removal of Cr (VI) in aqueous solution. *Journal of Solid State Chemistry*, Vol. 244, 2016, pp. 25–30.
- [68] Forghani, M., A. Azizi, M. J. Livani, and L. A. Kafshgari. Adsorption of lead (II) and chromium (VI) from aqueous environment onto metalorganic framework MIL-100 (Fe): Synthesis, kinetics, equilibrium and thermodynamics. *Journal of Solid State Chemistry*, Vol. 291, 2020, id. 121636.
- [69] Jalayeri, H., P. Aprea, D. Caputo, A. Peluso, and F. Pepe. Synthesis of amino-functionalized MIL-101 (Cr) MOF for hexavalent chromium adsorption from aqueous solutions. *Environmental Nanotechnology*, *Monitoring & Management*, Vol. 14, 2020, id. 100300.
- [70] Yang, Z.-h., J. Cao, Y.-p. Chen, X. Li, W.-p. Xiong, Y.-y. Zhou, et al. Mn-doped zirconium metal-organic framework as an effective adsorbent for removal of tetracycline and Cr (VI) from aqueous solution. Microporous and Mesoporous Materials, Vol. 277, 2019, pp. 277–285.
- [71] Guo, J., J.-J. Li, and C.-C. Wang. Adsorptive removal of Cr (VI) from simulated wastewater in MOF BUC-17 ultrafine powder. *Journal of Environmental Chemical Engineering*, Vol. 7, 2019, id. 102909.
- [72] Samuel, M. S., V. Subramaniyan, J. Bhattacharya, C. Parthiban, S. Chand, and N. P. Singh. A GO-CS@ MOF [Zn (BDC)(DMF)] material for the adsorption of chromium (VI) ions from aqueous solution. *Composites Part B: Engineering*, Vol. 152, 2018, pp. 116–125.
- [73] Li, X., X. Gao, L. Ai, and J. Jiang. Mechanistic insight into the interaction and adsorption of Cr (VI) with zeolitic imidazolate framework-67 microcrystals from aqueous solution. *Chemical Engineering Journal*, Vol. 274, 2015, pp. 238–246.
- [74] Niknam Shahrak, M., M. Ghahramaninezhad, and M. Eydifarash. Zeolitic imidazolate framework-8 for efficient adsorption and removal of Cr (VI) ions from aqueous solution. *Environmental Science and Pollution Research*, Vol. 24, 2017, pp. 9624–9634.
- [75] Maleki, A., B. Hayat, M. Naghizade, and S. W. Joo. Adsorption of hexavalent chromium by metal organic frameworks from aqueous solution. *Journal of Industrial and Engineering Chemistry*, Vol. 28, 2015, pp. 211–216.
- [76] Zhang, X., X. Lin, Y. He, Y. Chen, J. Zhou, and X. Luo. Adsorption of phosphorus from slaughterhouse wastewater by carboxymethyl konjac glucomannan loaded with lanthanum. *International Journal* of *Biological Macromolecules*, Vol. 119, 2018, pp. 105–115.
- [77] Lin, H., S. Han, Y. Dong, and Y. He. The surface characteristics of hyperbranched polyamide modified corncob and its adsorption property for Cr (VI). *Applied Surface Science*, Vol. 412, 2017, pp. 152–159.
- [78] Dong, L., J. Liang, Y. Li, S. Hunang, Y. Wei, X. Bai, et al. Effect of coexisting ions on Cr (VI) adsorption onto surfactant modified Auricularia auricula spent substrate in aqueous solution. *Ecotoxicology and Environmental Safety*, Vol. 166, 2018, pp. 390–400.
- [79] Hu, Z., L. Cai, J. Liang, X. Guo, W. Li, and Z. Huang. Green synthesis of expanded graphite/layered double hydroxides nanocomposites and their application in adsorption removal of Cr (VI) from aqueous solution. *Journal of Cleaner Production*, Vol. 209, 2019, pp. 1216–1227.

- [80] Jin, W., H. Du, S. Zheng, and Y. Zhang. Electrochemical processes for the environmental remediation of toxic Cr (VI): A review. *Electrochimica Acta*, Vol. 191, 2016, pp. 1044–1055.
- [81] Liu, F., S. Hua, C. Wang, M. Qiu, L. Jin, and B. Hu. Adsorption and reduction of Cr (VI) from aqueous solution using cost-effective caffeic acid functionalized corn starch. *Chemosphere*, Vol. 279, 2021, id. 130539.
- [82] Yang, Q., H. Wang, F. Li, Z. Dang, and L. Zhang. Rapid and efficient removal of Cr (vi) by a core–shell magnetic mesoporous polydopamine nanocomposite: roles of the mesoporous structure and redox-active functional groups. *Journal of Materials Chemistry A*, Vol. 9, 2021, pp. 13306–13319.
- [83] Xu, X., H. Huang, Y. Zhang, Z. Xu, and X. Cao. Biochar as both electron donor and electron shuttle for the reduction transformation of Cr (VI) during its sorption. *Environmental Pollution*, Vol. 244, 2019, pp. 423–430.
- [84] Liu, L., X. Liu, D. Wang, H. Lin, and L. Huang. Removal and reduction of Cr (VI) in simulated wastewater using magnetic biochar prepared by co-pyrolysis of nano-zero-valent iron and sewage sludge. *Journal of Cleaner Production*, Vol. 257, 2020, id. 120562.
- [85] Baskar, A. V., N. Bolan, S. A. Hoang, P. Sooriyakumar, M. Kumar, L. Singh, et al. Recovery, regeneration and sustainable management of spent adsorbents from wastewater treatment streams: A review. Science of the Total Environment, Vol. 822, 2022, id. 153555.

- [86] Haciosmanoğlu, G. G., C. Mejías, J. Martín, J. L. Santos, I. Aparicio, and E. Alonso. Antibiotic adsorption by natural and modified clay minerals as designer adsorbents for wastewater treatment: A comprehensive review. *Journal of Environmental Management*, Vol. 317, 2022, id. 115397.
- [87] Praveen, S., R. Gokulan, T. B. Pushpa, and J. Jegan. Techno-economic feasibility of biochar as biosorbent for basic dye sequestration. *Journal of the Indian Chemical Society*, Vol. 98, 2021, id. 100107.
- [88] Dobrzyńska, J., A. Wysokińska, and R. Olchowski. Raspberry stalks-derived biochar, magnetic biochar and urea modified magnetic biochar-Synthesis, characterization and application for As (V) and Cr (VI) removal from river water. *Journal of Environmental Management*, Vol. 316, 2022, id. 115260.
- [89] Bayuo, J., M. A. Abukari, and K. B. Pelig-Ba. Desorption of chromium (VI) and lead (II) ions and regeneration of the exhausted adsorbent. Applied Water Science, Vol. 10, 2020, id. 171.
- [90] Ogata, F., N. Nagai, R. Itami, T. Nakamura, and N. Kawasaki. Potential of virgin and calcined wheat bran biomass for the removal of chromium (VI) ion from a synthetic aqueous solution. *Journal of Environmental Chemical Engineering*, Vol. 8, 2020, id. 103710.
- [91] Bouchoum, H., D. Benmoussa, A. Jada, M. Tahiri, and O. Cherkaoui. Synthesis of amidoximated polyacrylonitrile fibers and its use as adsorbent for Cr (VI) ions removal from aqueous solutions. Environmental Progress & Sustainable Energy, Vol. 38, 2019, id. 13196.